Research Article

An investigation of the MHD Cu-Al$_2$O$_3$/H$_2$O hybrid-nanofluid in a porous medium across a vertically stretching cylinder incorporating thermal stratification impact

Ashish PAUL[1] , **Jintu MANI NATH[1,2],*** , **Tusar KANTI DAS[1]**

[1]Department of Mathematics, Cotton University, Guwahati, Assam, 781001, India
[2]Department of Mathematics, Mangaldai College, Mangaldai, Assam, 784125, India

ABSTRACT

The thermal aspects of $Cu - Al_2O_3/water$ hybrid nanofluid in a porous medium across a vertically stretched cylinder with the incorporation of heat sink/source impact are investigated in this numerical study. A magnetic field along the transverse direction of the stretching cylinder and the thermal buoyancy effect is considered in the flow problem. A pertinent similarity variable has been employed to simplify the boundary layer equations which govern the flow and convert the coupled nonlinear partial differential equations into a set of non-linear ordinary differential equations. The numerical results are computed using the 3-stage Lobatto IIIa technique, Bvp4c. The impacts of non- dimensional parameters, including Prandtl number, heat source/sink parameter, magnetic parameter, porosity parameter, curvature parameter, thermal stratification parameter, and thermal buoyancy parameter on the velocity curve, thermal curve, skin-friction coefficient, and Nusselt number, are illustrated graphically and numerically portrayed in tables. The important results demonstrate that hybrid nanofluids are more thermally conductive than nanofluids. Therefore, the hybrid nanofluid has a considerable impact on improving thermal developments. It has been found that the absolute skin friction of the hybrid nanofluid is up to 31% higher compared to the nanofluid. The heat transport rate of the hybrid nanofluid is 7.5% enhanced in comparison to the nanofluid. The influence of heat stratification of the hybrid nanofluid flow is appreciably significant.

Cite this article as: Paul A, Mani Nath J, Kanti Das T. An investigation of the MHD Cu-Al$_2$O$_3$/ H$_2$O hybrid-nanofluid in a porous medium across a vertically stretching cylinder incorporating thermal stratification impact. J Ther Eng 2023;9(3):799–810.

INTRODUCTION

New fluids, such as nanofluid, have been introduced in subsequent years to achieve considerable increases in thermal efficiency. Nanofluids are colloidal liquids with nanometer-sized components distributed throughout, which have unique characteristics that may make them effective in various heat transfer applications. Nanofluid has various thermal applications, including microfluidics,

---

pharmacological mechanisms, hybrid electric engines, private refrigerators, energy conversion, cooling systems, nuclear reactors, aerospace engineering, and defense.

A significant amount of research on nanofluid has already been published, particularly some intriguing phenomena, and many investigators have given theoretical and experimental conclusions. Yanijiao Li et al. [1] provided a brief overview of nanofluid creation and development. The unstable natural convection of a nanofluid across a vertical cylinder was explored by A.J. Chamkha et al. [2]. They also looked at how Brownian motion affects nanofluid movement. A review of magnetohydrodynamic nanofluid transient thermal efficiency in permeable medium was presented by Kasaeian et al. [3]. They concluded that employing nanofluid and porous media ameliorates the thermal transport rate in the system. After that, free-convection magnetohydrodynamic nanofluid with heat transport in a porous container was numerically analyzed by M. Sheikholeslami [4]. Isfahani et al. [5] investigated numerically and experimentally the Al_2O_3 nanofluid flow in the micro glass model, embedded in a permeable media by employing a pseudo-two-dimensional Lattice-Boltzmann Method. Using the lattice Boltzmann method, Mostafavi et al. [6] predicted the permeability of nano-porous structures. A.H. Meghdadi Isfahani [7] studied the rarefaction influences on micro- and nanoscale heat flows in the porous material. Zarei et al. [8] simulated the fluid flow in a nano-channel filled by a porous medium. By utilizing the analytic hierarchy methodology, Abdulvahitoglu [9] detected various kinds of nanofluids for the systems of engine cooling. Kilic et al. [10] investigated the thermal transmission numerically at a rectangular channel incorporating the impacts of swirling jets and nanofluids in a vehicle radiator. Recently, a mathematical solution for MHD Jeffery nanofluid flow across a vertical cylinder was provided by Hayat et al. [11].

Although nanofluid fulfills the engineer's and scientists' demands for thermal efficiency, a different kind of fluid is currently under investigation. Higher-level nanofluid, like "hybrid nanofluid," has been developed to address this. So, a hybrid nanofluid is a created nanofluid that has two different nanoparticles dispersed throughout the primary fluids. In order to prepare hybrid nanofluids, ethylene glycol, water, etc. are commonly utilized as the primary fluids, and Cu, Al_2O_3, MoS_2 etc., as the nanoparticles. It is a fluid invention that may upgrade thermal performance compared to regular coolant and nanofluid. High effective thermal conductivity, enhanced heat transfer, ascribed to the quality aspect ratio, and synergistic impact of nonmaterials are advantages of hybrid nanofluid. The utilization of hybrid nanofluid is in almost every discipline of heat transfer, such as solar heating, electronic cooling, nuclear system cooling, and transformer cooling, with greater capability than regular fluid and nanofluid. These favorable characteristics attract researchers to study on hybrid nanofluids in heat transport processes.

A major obstacle to the creation of energy-efficient heat transport fluids, which are crucial in numerous commercial processes, is poor thermal conductivity. By encapsulating metallic nanoparticles in traditional thermal transfer fluids, Choi and Eastman [12] proposed that a new and innovative class of heat transfer fluids could be created. Suresh et al. [13] investigated the impact of $Al_2O_3 - Cu/ H_2O$ hybrid nanofluid in heat transfer. They concluded that both the thermal conductivity and viscosity of the hybrid nanofluid were enhanced by the nanoparticle volume concentration. Labib et al. [14] numerically analyzed the importance of the base fluid and hybrid nanofluid on forced convective heat transfer. Momin [15] experimentally observed the water-Al_2O_3 and hybrid nanofluid mixed convection in an inclined tube. He reported that an enhancement in the particle volume concentration significantly lowers the experimental thermal transfer coefficient. The acceptable hybridization technique, effective for increasing heat transfer, was presented by Sarkar et al. [16]. Sundar et al. [17] discussed the thermal properties and preparation of a hybrid nanofluid. To prepare a hybrid nanofluid, one nanoparticle or nanotube need to be mixed with another nanoparticle that is immersed in a base fluid, like ethylene glycol, water, or other solvents so that the flow's fluidity is not affected.

Many researchers are curious about the steady stream of a viscous incompressible hybrid nanofluid across a vertical cylinder due to their engineering and earth sciences applications, including nuclear reactor cooling systems and underground power systems. Hot wires and ribbons, which are shaped like a vertical cylinder, are chilled as they traverse through the external environment in the optical and copolymer industries. A viscous fluid passed through a stretched cylinder in an axisymmetric mixed convective flow was discussed by Mukhopadhyay [18]. Gorla et al. [19] addressed the flow across a vertical cylinder immersed in a porous media saturated with a nanofluid. Najib et al. [20] observed the stagnation flow passed a shrinking and stretching cylinder. Later, across a vertically stretching cylinder, Rehman et al. [21] addressed the thermal properties and boundary layer flow of micro-polar fluid. By using the Buongiomo model, Rana et al. [22] analyzed the thermal effect and MHD slip flow of Al_2O_3-water nanofluid across a cylinder shrinking horizontally.

The superior thermal efficacy of hybrid nanofluid is illustrated by Devi and Devi [23]. They investigated numerically the hydromagnetic hybrid $Cu - Al_2O_3/H_2O$ nanofluid flow across the porous stretched sheet. Later, Devi and Devi [24] concluded that the Nusselt number is increased by up to 17.3% for $Cu - Al_2O_3$/water hybrid nanofluid. MHD flow across porous media is widely used in chemical, thermodynamic, and biological processes. Various researchers are only interested in that fluid flow because of its prospective scientific and technological applications, such as MHD turbines, nuclear reactors, and hydroelectric extraction. Waini et al. [25] investigated a hybrid nanofluid flow and

its impact over a non-linear permeable shrinking/ stretching surface. In Porous media, Ali et al. [26] analyzed the magneto-hydrodynamics hybrid $Cu - Al_2O_3/H_2O$ nanofluid flow incorporating thermal generation. They also discussed the impact of the induced magnetic field in their study. Biswas et al. [27] investigated the MHD heat convection of $Cu - Al_2O_3/H_2O$ hybrid nanofluid embedded in porous media along with half-sinusoidal nonuniform heating. Maskeen et al. [28], and Paul et al. [29] observed the increment in heat transfer in Al_2O_3—Cu/water-based hybrid nanofluid flow over a stretched cylinder. Yaskhun et al. [30] presented the impact of the magnetohydrodynamic flow in a porous mediuam of the hybrid nanofluid passed a shrinking/stretching sheet.

Later, Khashi'ie et al. [31] discussed the hybrid nanofluid flow over a shrinking cylinder by imposing surface heat flux. An investigation of the stability of the transient hybrid nanofluid flow over a porous shrinking/ stretching cylinder carried out by Zainal et al. [32]. Many scientists and researchers are interested in cylindrical geometry because of its vast range of uses. Waqas et al. [33] addressed the heat transport of hybrid nanofluids in a magnetized flow across a vertical stretched cylinder. Khashi'ie et al. [34] examined the hybrid nanofluid flow toward a vertical cylinder in a mixed convective stagnation point flow. By addressing the shape factor effect, Hosseinzadeh et al. [35] explored the fluid flow along a vertical cylinder. Recently, Swain et al. [36] discussed the impact of the variable magnetic field and chemical reaction of MWCNT/Fe_3O_4–water based hybrid nanofluid across a sheet that was shrinking exponentially by considering slip boundary conditions. Salahuddin et al. [37] addressed the 3D stagnation flow of a hybrid nanofluid flow near a highly magnetized heated stretching cylinder.

Scientists have extensively researched the influence that thermal and solute stratification performs on the transmission of heat and mass. Variations in liquid density, concentration, or temperature can cause stratification in flow fields. The thermal stratification phenomenon is utilized by seismic fluxes, groundwater reservoirs, and pond thermo-hydraulics. Deka and Paul [38-39] considered the buoyancy force when analyzing the transient flow across a vertical cylinder placed in a thermally stratified fluid. Using a hybrid nanoparticle, Khashi'ie et al. [40] discussed the thermally stratified flow through a porous stretching/ shrinking circular cylinder. The analysis showed that for both stretching and contracting cylinders, the stratification process influences the rate of thermal transmission. A thermally stratified hybrid nanofluid flow over a nonlinear extended surface was studied by Chung et al. [41]

Researchers have shown limited interest in studying the hybrid nanofluid flow over cylindrical geometry. Moreover, thermal stratification impact over linearly stretching cylinders has not been discussed elaborately in the literature. As per the review of the literature, no research has been published that investigates the impact of a heat source/ sink in a thermally stratified $Cu - Al_2O_3/Water$ MHD hybrid nanofluid flow immersed in a porous region over a vertically expanding cylinder by approaching the Bvp4c approach. The Bvp4c technique implemented in the present paper to simulate the problem is highly prevalent. The Bvp4c approach was discussed with examples in MATLAB by Shampine et al. [42] and Kierzenka et al. [43]. The governing set of non-linear PDEs is converted into a system of ODEs by a suitable transformation, and the solutions are solved using the Bvp4c techniques. The distinction between different parameters is shown graphically. The range of the Prandtl number is considered to be between 0.7 to 10. Again, the stratified thermal parameter is ranged from 0.05 to 0.5, whereas the value of the heat source/sink parameter is chosen as $-0.2 \leq S \leq 0.2$.

MATHEMATICAL FORMULATION

Consider a 2-dimensional steady incompressible $Cu - Al_2O_3/water$ hybrid nanofluid immersed in a porous space over a vertical stretchable cylinder in the presence of a heat source/sink. A magnetic field of strength B_0 is applied along the direction perpendicular to the propagation of the hybrid nanofluid, and the thermal buoyancy effect is considered in the flow problem. The velocity that stretches the vertical cylinder linearly is referred to as $u_w = a\frac{x}{l}$, where a and l illustrate the velocity and characteristic length of the cylinder. $T_w(x) = T_0 + A\left(\frac{x}{l}\right)$ is assumed to be wall temperature and $T_\infty(x) = T_0 + B\left(\frac{x}{l}\right)$ is the temperature of the hybrid nanofluid at the ambient; where A, B and T_0 illustrate non-negative constants and starting temperature, respectively.

Figure 1 shows a geometric representation of the hybrid nanofluid flow over a vertically stretching cylinder in a porous medium.
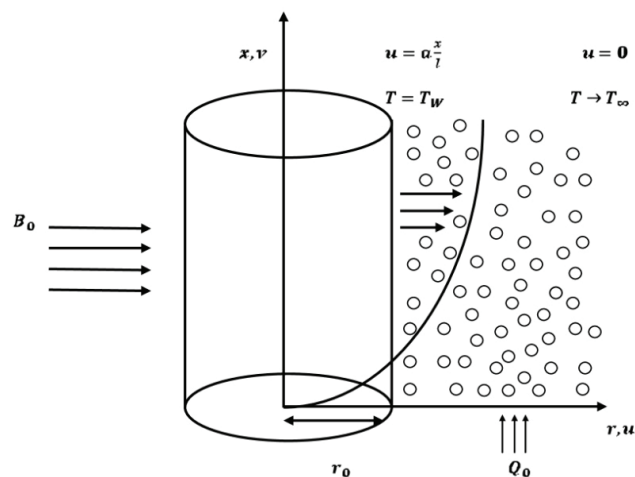

Figure 1. Flow diagram of the Mathematical model.

Considering the above assumptions, we can formulate the mathematical problem as follows (Ref. [40], [43]):

Continuity Equation

$$\frac{\partial(ru)}{\partial x} + \frac{\partial(rv)}{\partial r} = 0 \tag{1}$$

Momentum Equation

$$u\frac{\partial u}{\partial x} + v\frac{\partial u}{\partial r} = \frac{\mu_{hnf}}{\rho_{hnf}}\frac{1}{r}\frac{\partial}{\partial r}\left(r\frac{\partial u}{\partial r}\right) + \frac{(\rho\beta)_{hnf}}{\rho_{hnf}}g(T-T_\infty) - \frac{\sigma_{hnf}}{\rho_{hnf}}B_0{}^2 u - \frac{\mu_{hnf}}{\rho_{hnf}}\frac{u}{k} \tag{2}$$

Energy Equation

$$u\frac{\partial T}{\partial x} + v\frac{\partial T}{\partial r} = \frac{k_{hnf}}{(\rho c_p)_{hnf}}\frac{1}{r}\frac{\partial}{\partial r}\left(r\frac{\partial T}{\partial r}\right) + \frac{Q_0}{(\rho c_p)_{hnf}}(T-T_\infty) \tag{3}$$

With boundary conditions are as follows:

$$u = a\frac{x}{l} \ , \quad v = 0 \ , \quad T = T_w(x) \quad when \ r = r_0 \tag{4}$$

$$u = 0 \ , \quad T \to T_\infty(x) \qquad when \ r \to \infty \tag{5}$$

By imposing the following suitable similarity transformations (Ref. [40]) on Equations (1) - (3)

$$\eta = \frac{r^2 - r_0{}^2}{2r_0}\sqrt{\frac{a}{v_f l}} \ , \quad \psi = \sqrt{\frac{av_f}{l}}\,xr_0 f(\eta), \quad \theta = \frac{T - T_\infty(x)}{T_w(x) - T_0} \tag{6}$$

And considering the velocity components, $u = \frac{1}{r}\frac{\partial\psi}{\partial r}$, $v = -\frac{1}{r}\frac{\partial\psi}{\partial x}$, where ψ is stream function, we have the transformed equations reduced to

$$f'^2 - ff'' = Q_1(2\gamma f'' + (1+2\gamma\eta)f''') + Q_2\lambda\theta - (Q_3 M + Q_4 P)f' \tag{7}$$

$$f'(\theta + \delta) - f\theta' = Q_5\frac{1}{Pr}(2\gamma\theta' + (1+2\gamma\eta)\theta'') + Q_6 S\theta \tag{8}$$

And the corresponding transformed boundary conditions are as follows:

$$f(\eta) = 0, \quad f'(\eta) = 1, \quad \theta(\eta) = 1 - \delta \ \text{at} \ \eta = 0 \tag{9}$$

$$f'(\eta) \to 0, \quad \theta(\eta) \to 0 \ \text{as} \ \eta \to \infty \tag{10}$$

Where

$$Q_1 = \frac{\mu_{hnf}}{\mu_f}\frac{\rho_f}{\rho_{hnf}}, \quad Q_2 = \frac{(\rho\beta)_{hnf}}{(\rho\beta)_f}\frac{\rho_f}{\rho_{hnf}},$$

$$Q_3 = \frac{\sigma_{hnf}}{\sigma_f}\left(\frac{\rho_f}{\rho_{hnf}}\right), \quad Q_4 = \frac{\mu_{hnf}}{\mu_f}\left(\frac{\rho_f}{\rho_{hnf}}\right),$$

$$Q_5 = \frac{k_{hnf}}{k_f}\frac{(\rho c_p)_f}{(\rho c_p)_{hnf}} \ , \quad Q_6 = \frac{(\rho c_p)_f}{(\rho c_p)_{hnf}}$$

And the non-dimensional parameters are specified as follows:

$$M = \frac{B_0{}^2 l\sigma_f}{a\rho_f} \ , \quad P = \frac{l}{a}\frac{\vartheta_f}{k} \ , \quad \gamma = \sqrt{\frac{l\vartheta_f}{ar_0{}^2}} \ , \quad \lambda = \frac{Gr_x}{Re_x{}^2},$$

$$\delta = \frac{B}{A} \ , \quad S = \frac{Q_0 l}{(\rho c_p)_f a} \ , \quad Pr = \frac{\vartheta_f(\rho c_p)_f}{k_f}$$

The density ρ_{hnf}, thermal conductivity k_{hnf}, thermal expansion $(\rho\beta_T)_{hnf}$, dynamic viscosity μ_{hnf}, heat capacity $(\rho C_p)_{hnf}$ of hybrid nanofluid are defined as follows (Ref. [24], [40]) :

$$\rho_{hnf} = (1-\phi_2)\{(1-\phi_1)\rho_f + \phi_1\rho_{s1}\} + \phi_2\rho_{s2} \tag{11}$$

$$k_{hnf} = k_{bf}\left\{\frac{k_{s2}+2k_{bf}-2\phi_2(k_{bf}-k_{s2})}{k_{s2}+2k_{bf}+\phi_2(k_{bf}-k_{s2})}\right\} \tag{12}$$

Where $k_{bf} = k_f\left\{\frac{k_{s1}+2k_f-2\phi_1(k_f-k_{s1})}{k_{s1}+2k_f+\phi_1(k_f-k_{s1})}\right\}$,

$$(\rho\beta_T)_{hnf} = (1-\phi_2)\{(1-\phi_1)(\rho\beta_T)_f + \phi_1(\rho\beta_T)_{s1}\} + \phi_2(\rho\beta_T)_{s2} \tag{13}$$

$$\mu_{hnf} = \mu_f(1-\phi_1)^{-2.5}(1-\phi_2)^{-2.5} \tag{14}$$

$$(\rho C_p)_{hnf} = (1-\phi_2)\left\{(1-\phi_1)(\rho C_p)_f + \phi_1(\rho C_p)_{s1}\right\} + \phi_2(\rho C_p)_{s2} \tag{15}$$

Thermo-physical characteristics of Cu and Al_2O_3 nanoparticles in pure water are presented in Table 1. (see Devi and Devi [24], Khashi'ie et al. [40])

The skin friction coefficient and local Nusselt number are defined by

$$C_f Re_x{}^{1/2} = \frac{1}{(1-\phi_1)^{2.5}(1-\phi_2)^{2.5}}f''(0) \tag{16}$$

$$Nu_x Re_x{}^{-1/2} = -\frac{k_{hnf}}{k_f}\theta'(0) \tag{17}$$

Where Re_x is the local Reynolds number.

Table 1. Thermo-physical features of the alumina, copper, and water

Properties	ρ (kg/m^3)	C_p (J/ kg K)	k (W/ mK)	β_T (K^{-1})
Alumina	3970	765	40	0.85 x 10^{-5}
Copper	8933	385	400	1.67 x 10^{-5}
Water	997.1	4179	0.6130	21 x 10^{-5}

METHOD OF SOLUTION

The function bvp4c is employed to numerically demonstrate the coupled higher order ordinary differential equations (7)–(8), subject to the constraints given in equations (9) and (10), for distinct values of the physical parameters Prandtl number, heat source/sink parameter, Magnetic parameter, Porosity parameter, Curvature parameter, Thermal stratification parameter, and Thermal buoyancy parameter. The three phases of the Lobatto IIIa formula are implemented using the MATLAB BVP solver, bvp4c, which is a finite difference code. Using bvp4c from MATLAB, equations (1) to (3) are transformed into a system of first-order equations. The explanation of the bvp4c approach is given by Shampine et al. [41]. Now, letting $[y(1)\ y(2)\ y(3)\ y(4)\ y(5)]T = [f\ f'\ f''\theta\ \theta']T$ provides

$$\frac{d}{d\eta}\begin{pmatrix} y(1) \\ y(2) \\ y(3) \\ y(4) \\ y(5) \end{pmatrix} = \begin{pmatrix} y(2) \\ y(3) \\ \left(\frac{1}{1+(2*\gamma*\eta)}\right)*\left(\left(\frac{1}{Q_1}\right)*\left(y(2)^2 - y(1)*y(3) - Q_2*\lambda*y(4) + (Q_3*M + Q_4*P)*y(2)\right) - 2*\gamma*y(3)\right) \\ y(5) \\ \left(\frac{1}{1+(2*\gamma*\eta)}\right)*\left(\left(\frac{Pr}{Q_5}\right)*\left(y(2)*y(4) + y(2)*\delta - y(1)*y(5) - Q_6*S*y(4)\right) - 2*\gamma*y(5)\right) \end{pmatrix}$$

RESULTS AND DISCUSSIONS

This investigation deals with water-based $Cu - Al_2O_3$ hybrid nanofluid flow with nanoparticles volume fraction range from 0.03 to 0.1 incorporating thermal buoyancy impact with the magneto-hydrodynamic flux over a vertically stretching cylinder. The importance of MHD flux can be eyed on the industrial field, such as MHD power pumps, MHD generators, etc. The impact of a heat source/ sink is also addressed due to its immense applications in microelectronic gadgets; as a coolant, and even in the nuclear reactor. Due to the appreciable and significant applications of the thermal stratification factor in the field of heat transmission, it is also added to the flow model. Further, by adopting the MATLAB- based Bvp4c technique, the concurrent mathematical model is solved for various values of non- dimensional flow parameters, namely, heat source/sink, thermal stratification, porosity, Prandtl number, magnetic, thermal buoyancy, and the curvature. The numerical solutions are also depicted through graphs and tables by treating the volume fraction of Cu nanoparticle as 0.1, which is immersed in a 0.05 volume fraction of alumina.

In Table 2, values of $-\theta'(0)$ obtained by this investigation are contrasted to those reported by Ishak and Nazar [44] and Elbashbeshy et al. [45], in the exclusion of nanoparticle volume fractions with $\gamma = 0$, $M = 0$, $\delta = 0$, $P = 0$, $S = 0$, $\lambda = 0$ and varying Prandtl number values. It demonstrates that the bvp4c algorithm can provide numerical findings that are precise and consistent with the outcomes of the other approaches.

Table 2. Comparable values of $-\theta'(0)$ with M = P = γ = δ = S = λ = ϕ_1 = ϕ_2 = 0 and various values of Prandtl number

Pr	Ishak and Nazar [44]	Elbashbeshy et al. [45]	Present Study
1	1.0000	1.0000	1.0005
10	3.7207	3.7207	3.7200

Figures 2 and 3, respectively, illustrate how the heat source/sink parameter, S, affects the velocity and thermal profiles. It is detected that when the heat source parameter is enhanced, the velocity curve escalates, and the curve tends to move down when the heat sink parameter is increased. The same pattern is also observed for the profile of heat distribution. It is because when the heat source is raised, more heat is added to the vertical surface of the stretching cylinder, which results in enhanced heat boundary layer thickness. On the other hand, an enhanced heat sink specifies that more heat is absorbed from the vertical surface of the stretching cylinder, which leads to the declination of the temperature profile, as shown in Figure 3.
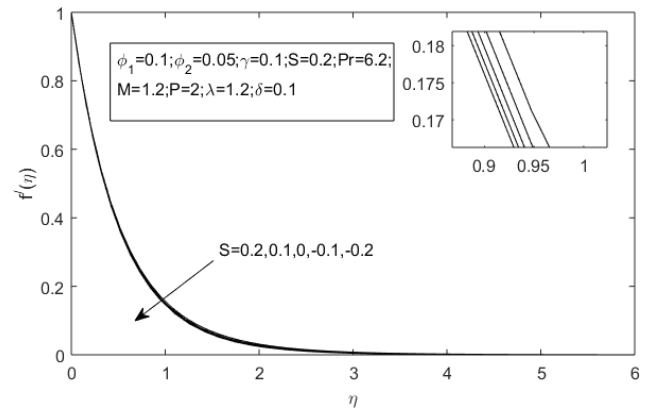

Figure 2. Impact of heat source/sink parameter on the velocity profile.
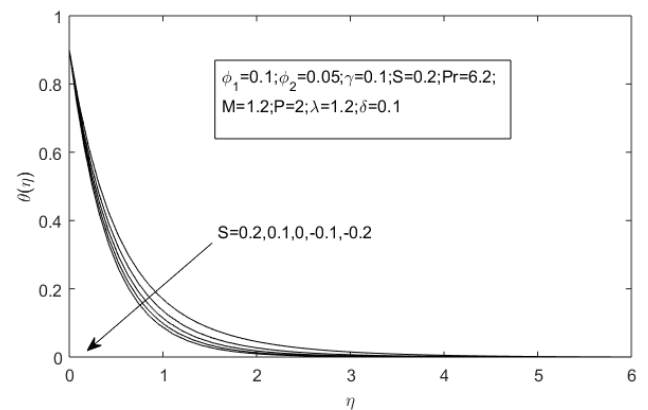

Figure 3. Impact of heat source/sink parameter on temperature profile.

The influence of the magnetic intensity, M, on the thermal and velocity profiles is reflected in Figures 4 and 5. With a rising level of the magnetic parameter, the flow velocity considerably reduces throughout the fluid region. When a material is subjected to an electrically conducting fluid, it exerts a drag-like force referred to as the Lorentz force. Because the magnetic flux opposes the transport phenomena, this force causes a drop in flow speed within the boundary layer. The thermal distribution grows as the magnetic field effect raises. The Lorentz force's impact on velocity distribution created friction in the stream, which released more thermal energy, resulting in an improvement in the temperature distribution in the flow.
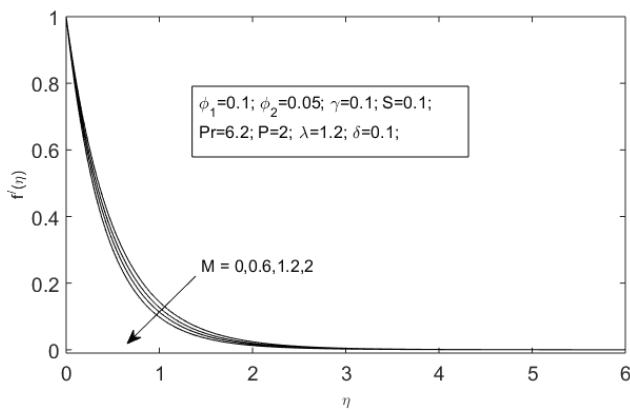

Figure 6. Impact of Prandtl number on the velocity profile.

Figure 4. Impact of Magnetic parameter on the velocity profile.

Figure 7. Impact of Prandtl number on the temperature profile.

Figures 8 and 9 show the impact of the porosity on the velocity and the thermal curves, respectively. As P is inversely proportional to the diameter of the porous space, while P increases, the diameter of the porous space gradually reduces, which does not easily allow the fluid to pass through the porous space. Due to this hindrance caused by P, fluid velocity decreased, but the temperature profile showed the opposite trend as P increased.
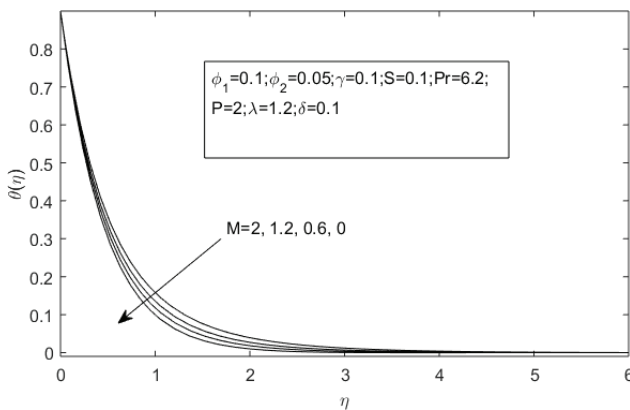

Figure 5. Impact of Magnetic parameter on the temperature profile.

Figures 6 and 7 demonstrate the impact of the Prandtl number on velocity and thermal profile. With the increase of the Prandtl number, the velocity profile seems to decelerate. It has been spotted that increasing the Prandtl number lessens the thickness of the heat boundary layer, leading to a reduction in the temperature curve.
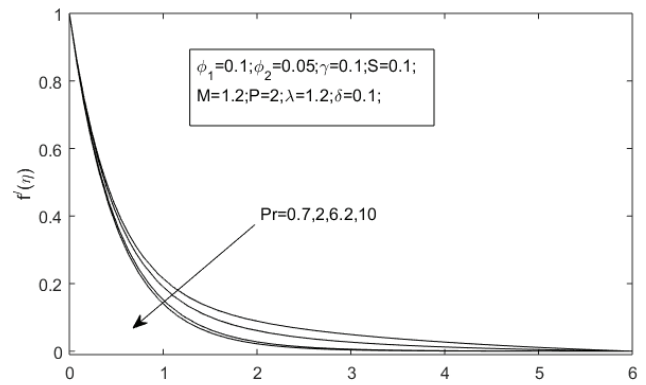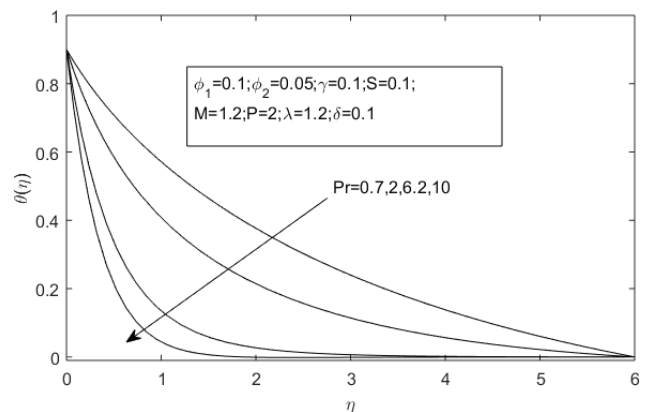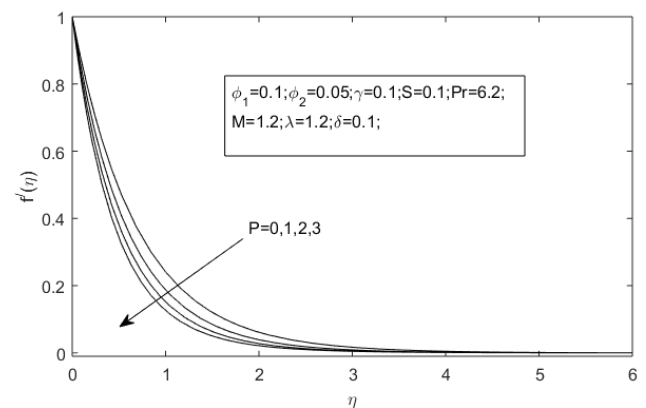

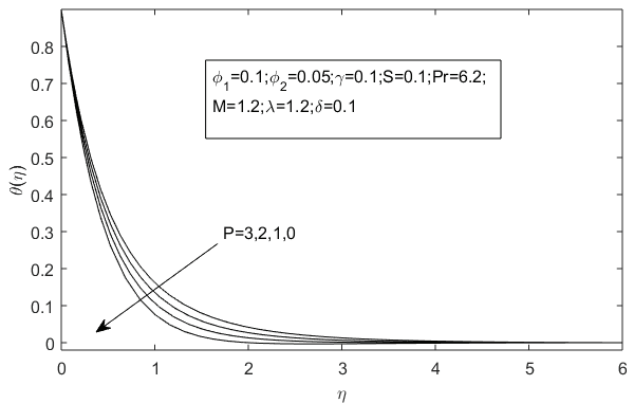**Figure 8.** Impact of Porosity parameter on the velocity profile.

Figure 9. Impact of Porosity parameter on the temperature profile.

Figures 10 and 11 depict the velocity and temperature with a rise of the heat buoyancy parameter, λ. The heat buoyancy parameter is proportional to the Grashof number Gr_x, that refers to the ratio of buoyancy force to viscous force. As λ increases, Gr_x raises, which leads to a lessening in the viscous force, and so the velocity profile increases. Gr_x is used to characterize the fluid inertia effect, and a rise in the inertia force parameter reduces the heat boundary layer thickness. As λ increases, Gr_x also enhances, and so inertia force decreases. This results in the boundary layer thickness getting thinner, and also the heat profile is narrowed.

The influence of the curvature parameter, γ is depicted in Figures 12 and 13. An upsurge in the values of γ increases the velocity while the temperature profile is observed to be reduced. Figures 14 and 15 show the trend of velocity and temperature distribution for the thermal stratification parameter, δ. It is noticed that thermal stratification diminishes the velocity in the boundary layer. The thermal stratification will minimizes the effective convective potential between the ambient fluid and the heated wall. Moreover, thermal stratification operates as a resistive force; it has a layering effect that contributes to the drop in velocity. Figure 15 illustrates that as thermal stratification rises, the temperature falls. Also, the dimensionless temperature
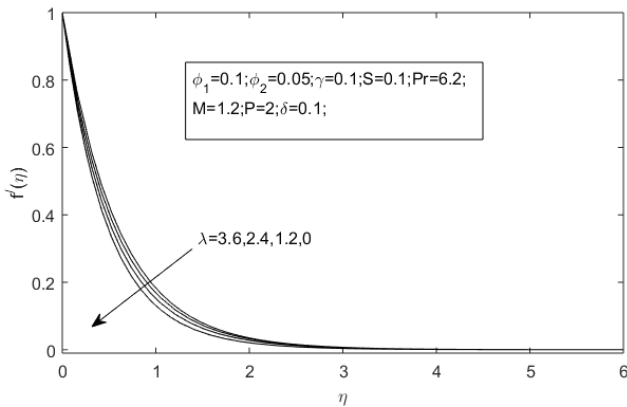

Figure 10. Impact of Thermal buoyancy parameter on the velocity profile.
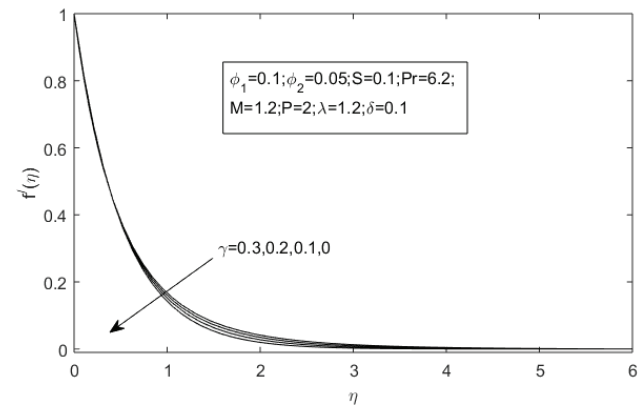

Figure 12. Impact of curvature parameter on the velocity profile.
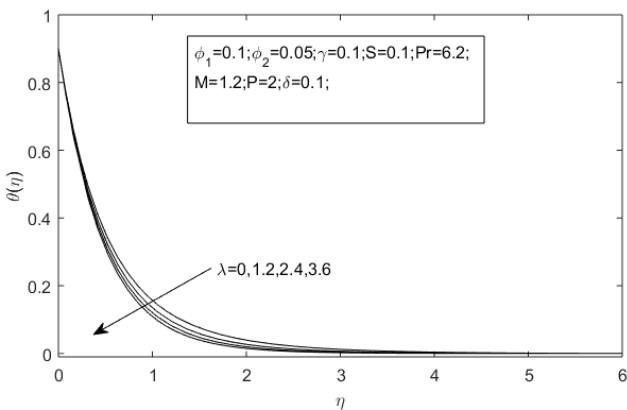

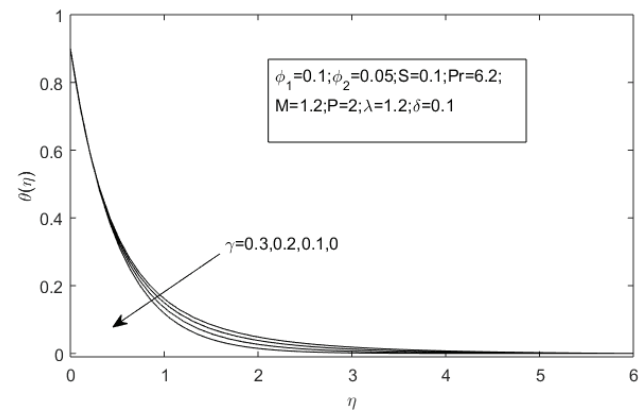**Figure 11.** Impact of Thermal buoyancy parameter on the temperature profile.

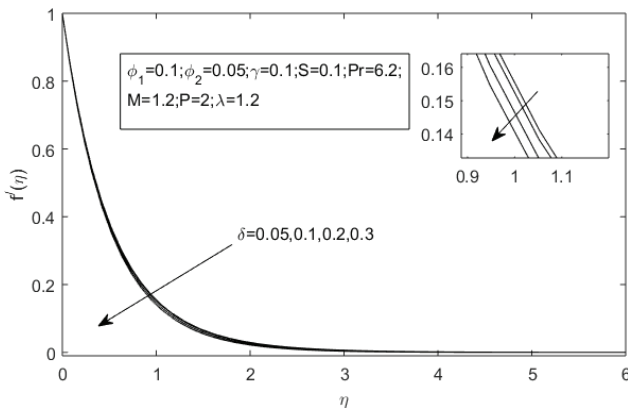**Figure 13.** Impact of curvature parameter on the temperature profile.

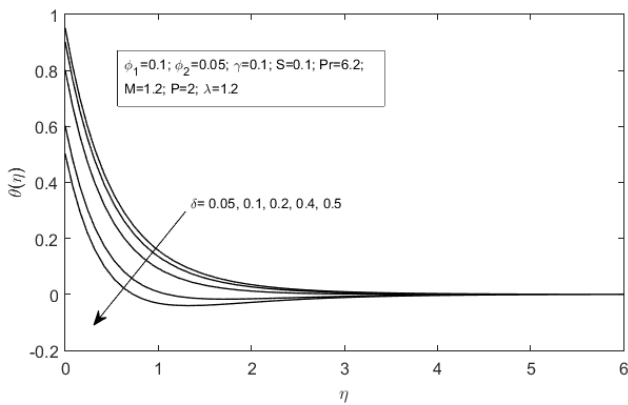**Figure 14.** Impact of thermal stratification parameter on the velocity profile.

Figure 15. Impact of thermal stratification parameter on temperature profile.
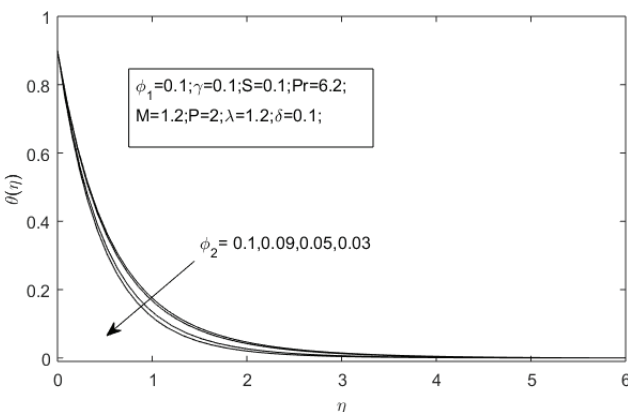

Figure 16. Impact of volume fraction of Cu on the temperature profile.

becomes negative when there is high thermal stratification because the fluid close to the cylinder may have a temperature lower than the ambient.

As the solid volume fraction of Cu nanoparticle enhances, while the volume fraction of Al_2O_3 is keeping constant, the thermal profile also grows, as depicted in Fig 16. Also, while the volume fraction of Cu is kept constant, the thermal curve is enhanced for the rising volume fraction of Al_2O_3 as depicted in Figure 17.
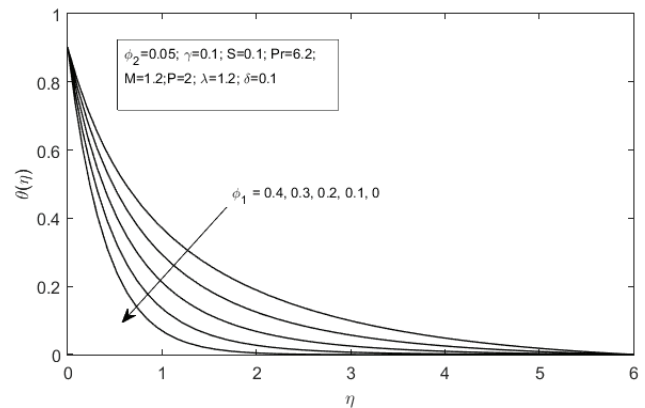
Figure 17. Impact of volume fraction of Al_2O_3 on the temperature profile.

The impact on skin friction and Nusselt number for different flow parameters is illustrated in Tables 3 and Table 4. A rise in the absolute value of skin friction and Nusselt number is noted with increasing Pr. Declination in the rate of heat transfer is seen for increasing M, whereas the reverse is the trend for absolute values of skin friction with an increase in M. As the porosity parameter P increases, the absolute skin friction number is enhanced, whereas the heat transfer flow accelerates in the opposite direction.

Table 3. Variation in skin friction and Nusselt numbers while $\gamma = 0.1$, $S = 0.1$, $\lambda = 1.2$, $\delta = 0.1$

Pr	M	P	skin-friction	Nusselt Number
0.7	1.2	2	2.7886	0.7266
2			2.8419	1.3264
6.2			2.9398	2.7885
10			2.9833	3.7670
6.2	0	2	2.4556	2.9414
	0.6		2.7076	2.8622
	1.2		2.9398	2.7885
	2		3.2255	2.6969
6.2	1.2	0	2.1201	3.0458
		1	2.5598	2.9087
		2	2.9398	2.7885
		3	3.2793	2.6795

Table 4. Variation in skin friction and Nusselt numbers while Pr = 6.2, M = 1.2, P = 2

S	δ	λ	γ	skin-friction	Nusselt Number
-0.2	0.1	1.2	0.1	2.9620	3.2685
-0.1				2.9560	3.1231
0				2.9488	2.9651
0.1				2.9398	2.7885
0.2				2.9270	2.5773
0.1	0.05	1.2	0.1	2.9213	2.8338
	0.1			2.9398	2.7885
	0.2			2.9767	2.6964
	0.3			3.0135	2.6025
0.1	0.1	0	0.1	3.1690	2.7064
		1.2		2.9398	2.7885
		2.4		2.7219	2.8528
		3.6		2.5117	2.9072
0.1	0.1	1.2	0	2.8737	2.7497
			0.1	2.9398	2.7885
			0.2	3.0048	2.8283
			0.3	3.0689	2.8697

With increasing values of *S*, both shear stress and Nusselt number are reduced. On the other hand, a reduction in the heat transfer rate is noticed for rising values of δ, but the opposite is the pattern in the case of skin friction. For λ, findings are vice-versa with the results obtained for δ. Absolute Skin friction decreases while the Nusselt number increases for λ. An upsurge in both absolute skin friction and the thermal transfer rate is observed for the curvature parameter γ.

The absolute skin friction and the Nusselt number are found to be improved with an enhancement in the volume concentration of *Cu* nanoparticles while maintaining ϕ_1 at zero in table 5. Moreover, it has been determined that when the volume concentration of Al_2O_3 is set to 0.1, the rate of heat transfer climbs by more than 7.5%. Based on the above findings, it is clear that hybrid nanofluid has a

thermal transmission rate that is noticeably greater than that of nanofluid. Also, the absolute skin friction of the hybrid nanofluid is shown to be enhanced by more than 31%.

CONCLUSIONS

The influences of momentum and thermal boundary layer of MHD hybrid nanofluid flow over a vertical stretchable cylinder with a bouncy effect, incorporating the heat source/sink impact embedded in a porous space, have been explored thoroughly. A parametric investigation has been carried out to have a detailed and crystal clear physical understanding of the problem. The flow parameters and their impacts on the velocity curve and thermal curve, skin friction drag force, and Nusselt number are also analyzed. The prime findings of the present study are mentioned below:

- The absolute skin friction is enhanced for all non-dimensional parameters except for λ and S.
- An enhancement in the heat transport rate is detected for increasing values of γ, λ, Pr.
- The velocity profile slows down for incremented M, Pr, P, and δ, but increases when λ and γ increase.
- The heat transport rate is found to be decelerated for increasing δ, M, S, and P.
- The absolute value of the skin friction for $Cu - Al_2O_3/water$ hybrid nanofluid is enhanced by up to 31% when compared with $Cu - water$ nanofluid.
- The Nusselt number is also found to be increased for $Cu - Al_2O_3/water$ hybrid nanofluid by more than 7.5% when compared with $Cu - water$ nanofluid. Hybrid nanofluid has a thermal transmission rate that is noticeably greater than that of nanofluid.

NOMENCLATURE

$(C_p)_f$	Fluid specific heat capacity ($J\ kg^{-1}K^{-1}$)
$(C_p)_{hnf}$	Hybrid nanofluid specific heat capacity ($J\ kg^{-1}K^{-1}$)
$(C_p)_{s1}$	Specific heat capacity of the Al_2O_3 ($J\ kg^{-1}K^{-1}$)
$(C_p)_{s2}$	Specific heat capacity of the Cu ($J\ kg^{-1}K^{-1}$)
Gr_x	Grashof number
k_f	Thermal conductivity of the fluid ($Wm^{-1}K^{-1}$)

Table 5. Comparison of the skin friction coefficient and Nusselt number for Cu/H$_2$O nanofluid and Cu − Al$_2$O$_3$/H$_2$O hybrid nanofluid.

		Cu/H_2O				$Cu - Al_2O_3/H_2O$		Change in %	
ϕ_1	ϕ_2	Skin Friction Coefficient	Nusselt Number	ϕ_1	ϕ_2	Skin Friction Coefficient	Nusselt Number	Skin Friction Coefficient	Nusselt Number
0	0.03	2.0751	2.5432	0.1	0.03	2.7699	2.7458	33.4	7.9
	0.05	2.2127	2.5856		0.05	2.9398	2.7885	32.8	7.8
	0.09	2.5109	2.6695		0.09	3.3101	2.8723	31.8	7.6
	0.1	2.5907	2.6903		0.1	3.4098	2.8930	31.6	7.5

k_{bf}	Thermal conductivity of the nanofluid ($Wm^{-1}K^{-1}$)
k_{hnf}	Thermal conductivity of the hybrid nanofluid ($Wm^{-1}K^{-1}$)
k_{s1}, k_{s2}	Thermal conductivity of the solid nanoparticles ($Wm^{-1}K^{-1}$)
k	Permeability of porous media (m^2)
M	Magnetic parameter
P	Porosity parameter
Pr	Prandtl Number
Re_x	Local Reynolds number
S	Heat source/sink parameter
T	Fluid temperature (K)
T_∞	Ambient fluid temperature (K)
T_w	Wall temperature (K)
u	Velocity component along r directions (ms^{-1})
v	Velocity component along x directions (ms^{-1})
B_0	Magnetic field strength (NmA^{-1})
Q_0	Heat source/sink ($JK^{-1}m^{-3}s^{-1}$)

Greek symbols

ψ	Stream function
ϕ_1, ϕ_2	The volume fraction of Al_2O_3 and Cu
ρ_{s1}	Density of Al_2O_3 (kgm^{-3})
ρ_{s2}	The density of Cu (kgm^{-3})
ρ_f	The density of the fluid (kgm^{-3})
ρ_{hnf}	The density of the hybrid nanofluid (kgm^{-3})
γ	The curvature parameter
δ	Thermal stratification parameter
η	Similarity variable
λ	Thermal buoyancy parameter
μ_f	Dynamic viscosity of the fluid (mPa)
μ_{hnf}	Dynamic viscosity of hybrid nanofluid (mPa)
σ_{hnf}	The electric conductivity of hybrid nanofluid ($Ohm^{-1}m^{-1}$)
$(\beta_T)_f$	Thermal expansion of the fluid (K^{-1})
$(\beta_T)_{s1}$	Thermal expansion of the Al_2O_3 (K^{-1})
$(\beta_T)_{s2}$	Thermal expansion Cu (K^{-1})

Subscripts

f	Fluid
bf	Nanofluid
hnf	Hybrid nanofluid
s	Solid

AUTHORSHIP CONTRIBUTIONS

Authors equally contributed to this work.

DATA AVAILABILITY STATEMENT

The authors confirm that the data that supports the findings of this study are available within the article. Raw data that support the finding of this study are available from the corresponding author, upon reasonable request.

CONFLICT OF INTEREST

The author declared no potential conflicts of interest with respect to the research, authorship, and/or publication of this article.

ETHICS

There are no ethical issues with the publication of this manuscript.

REFERENCES

[1]   Li Y, Tung S, Schneider E, Xi S. A review on development of nanofluid preparation and characterization. Powder Technol 2009;196:89–101. [CrossRef]

[2]   Chamkha AJ, Rashad AM, Aly AM. Transient natural convection flow of a nanofluid over a vertical cylinder. Meccanica 2013;48:71–81. [CrossRef]

[3]   Kasaeian A, Daneshazarian R, Mahian O, Kolsi L, Chamkha AJ, Wongwises S, et al. Nanofluid flow and heat transfer in porous media: a review of the latest developments. Int J Heat Mass Transf 2017;107:778–791. [CrossRef]

[4]   Sheikholeslami M. Numerical investigation of MHD nanofluid free convective heat transfer in a porous tilted enclosure. Eng Comput 2017;34:1939–1955. [CrossRef]

[5]   Isfahani AM, Afrand M. Experiment and Lattice Boltzmann numerical study on nanofluids flow in a micromodel as porous medium. Physica E Low Dimens 2017;94:15–21. [CrossRef]

[6]   Mostafavi M, Meghdadi Isfahani AH. A new formulation for prediction of permeability of nano porous structures using lattice botzmann method. J Appl Fluid Mech 2017;10:639–649. [CrossRef]

[7]   Meghdadi Isfahani AH. Parametric study of rarefaction effects on micro-and nanoscale thermal flows in porous structures. J Heat Transf 2017;139:092601. [CrossRef]

[8]   Zarei A, Karimipour A, Isfahani AH, Tian Z. Improve the performance of lattice Boltzmann method for a porous nanoscale transient flow by provide a new modified relaxation time equation. Phys A Stat Mech Appl 2019;535:122453. [CrossRef]

[9]   Abdulvahitoglu A. Using analytic hierarchy process for evaluating different types of nanofluids for engine cooling systems. Therm Sci 2019;23:3199–3208. [CrossRef]

[10]   Kilic M, Abdulvahitoglu A. Numerical investigation of heat transfer at a rectangular channel with combined effect of nanofluids and swirling jets in a vehicle radiator. Therm Sci 2019;23:3627–3637. [CrossRef]

[11]   Hayat T, Ullah H, Ahmad B, Alhodaly MS. Heat transfer analysis in convective flow of Jeffrey nanofluid by vertical stretchable cylinder. Int Commun Heat Mass Transf 2021;120:104965. [CrossRef]

[12] Choi SU, Eastman JA. Enhancing thermal conductivity of fluids with nanoparticles. Argonne National Lab(ANL), Argonne, IL (United States); 1995.

[13] Suresh S, Venkitaraj KP, Selvakumar P, Chandrasekar M. Synthesis of Al_2O_3-Cu/water hybrid nanofluids using two step method and its thermo physical properties. Colloids Surf A Physicochem Eng Asp 2011;388:41−48. [CrossRef]

[14] Labib MN, Nine MJ, Afrianto H, Chung H, Jeong H. Numerical investigation on effect of base fluids and hybrid nanofluid in forced convective heat transfer. Int J Therm Sci 2013;71:163−171. [CrossRef]

[15] Momin GG. Experimental investigation of mixed convection with water-Al2O3 & hybrid nanofluid in inclined tube for laminar flow. Int J Sci Technol Res 2013;2:195−202.

[16] Sarkar J, Ghosh P, Adil A. A review on hybrid nanofluids: recent research, development and applications. Renew Sustain Energy Rev 2015;43:164−177. [CrossRef]

[17] Sundar LS, Sharma KV, Singh MK, Sousa AC. Hybrid nanofluids preparation, thermal properties, heat transfer and friction factor-a review. Renew Sustain Energy Rev 2017;68:185−198. [CrossRef]

[18] Mukhopadhyay S. Mixed convection boundary layer flow along a stretching cylinder in porous medium. J Pet Sci Eng 2012;96:73−78. [CrossRef]

[19] Gorla RS, Hossain A. Mixed convective boundary layer flow over a vertical cylinder embedded in a porous medium saturated with a nanofluid. Int J Numer Methods Heat Fluid Flow. 2013;23:1393−1405. [CrossRef]

[20] Najib N, Bachok N, Arifin NM, Ishak A. Stagnation point flow and mass transfer with chemical reaction past a stretching/shrinking cylinder. Sci Rep 2014;4:1−7. [CrossRef]

[21] Rehman A, Bazai R, Achakzai S, Iqbal S, Naseer M. Boundary layer flow and heat transfer of micropolar fluid over a vertical exponentially stretched cylinder. App Comp Math 2015;4:424−430. [CrossRef]

[22] Rana P, Dhanai R, Kumar L. MHD slip flow and heat transfer of Al2O3-water nanofluid over a horizontal shrinking cylinder using Buongiorno's model: Effect of nanolayer and nanoparticle diameter. Adv Powder Technol 2017;28:1727−1738. [CrossRef]

[23] Devi SA, Devi SS. Numerical investigation of hydromagnetic hybrid Cu-Al_2O_3/water nanofluid flow over a permeable stretching sheet with suction. Int J Nonlinear Sci Numer Simul 2016;17:249−257. [CrossRef]

[24] Devi SU, Devi SA. Heat transfer enhancement of Cu-Al_2O_3/water hybrid nanofluid flow over a stretching sheet. J Niger Soc Math Biol 2017;36:419−433.

[25] Waini I, Ishak A, Pop I. Hybrid nanofluid flow and heat transfer over a nonlinear permeable stretching/shrinking surface. Int J Numer Methods Heat Fluid Flow. 2019;29:3110−3127. [CrossRef]

[26] Ali K, Ahmad S, Nisar KS, Faridi AA, Ashraf M. Simulation analysis of MHD hybrid Cu Al_2O_3/H_2O nanofluid flow with heat generation through a porous media. Int J Energy Res 2021;45:19165−19179. [CrossRef]

[27] Biswas N, Sarkar UK, Chamkha AJ, Manna NK. Magneto-hydrodynamic thermal convection of Cu-Al2O3/water hybrid nanofluid saturated with porous media subjected to half-sinusoidal nonuniform heating. J Therm Anal Calorim 2021;143:1727−1753. [CrossRef]

[28] Maskeen MM, Zeeshan A, Mehmood OU, Hassan M. Heat transfer enhancement in hydromagnetic alumina-copper/water hybrid nanofluid flow over a stretching cylinder. J Therm Anal Calorim 2019;138:1127−1136. [CrossRef]

[29] Paul A, Das TK, Nath JM. Numerical investigation on the thermal transportation of MHD Cu/Al_2O_3-H_2O Casson-hybrid-nanofluid flow across an exponentially stretching cylinder incorporating heat source. Phys Scr 2022;28:085701. [CrossRef]

[30] Yashkun U, Zaimi K, Bakar NA, Ishak A, Pop I. MHD hybrid nanofluid flow over a permeable stretching/shrinking sheet with thermal radiation effect. Int J Numer Methods Heat Fluid Flow 2020;31. [CrossRef]

[31] Khashi'ie NS, Waini I, Zainal NA, Hamzah K, Mohd Kasim AR. Hybrid nanofluid flow past a shrinking cylinder with prescribed surface heat flux. Symmetry 2020;12:1493. [CrossRef]

[32] Zainal NA, Nazar R, Naganthran K, Pop I. Stability analysis of unsteady hybrid nanofluid flow past a permeable stretching/shrinking cylinder. J Adv Res Fluid Mech Therm Sci 2021;86:64-75. [CrossRef]

[33] Waqas H, Naqvi SM, Alqarni MS, Muhammad T. Thermal transport in magnetized flow of hybrid nanofluids over a vertical stretching cylinder. Case Stud Therm Eng 2021;27:101219. [CrossRef]

[34] Khashi'ie NS, Arifin NM, Merkin JH, Yahaya RI, Pop I. Mixed convective stagnation point flow of a hybrid nanofluid toward a vertical cylinder. Int J Numer Meth Heat Fluid Flow 2021;31. [CrossRef]

[35] Hosseinzadeh K, Asadi A, Mogharrebi AR, Ermia Azari M, Ganji DD. Investigation of mixture fluid suspended by hybrid nanoparticles over vertical cylinder by considering shape factor effect. Journal of Therm Anal Calorim 2021;143:1081−1095. [CrossRef]

[36] Swain K, Mebarek-Oudina F, Abo-Dahab SM. Influence of MWCNT/Fe_3O_4 hybrid nanoparticles on an exponentially porous shrinking sheet with chemical reaction and slip boundary conditions. J Therm Anal Calorim 2022;147:1561−1570. [CrossRef]

[37] Salahuddin T, Siddique N, Khan M, Chu YM. A hybrid nanofluid flow near a highly magnetized heated wavy cylinder. Alex Eng J 2022;61:1297−1308. [CrossRef]

[38]   Deka RK, Paul A. Transient free convection flow past an infinite vertical cylinder with thermal stratification. J Mech Sci Technol 2012;26:2229−2237. [CrossRef]

[39]   Deka RK, Paul A. Transient free convection flow past an infinite moving vertical cylinder in a stably stratified fluid. J Heat Trans 2012;134:042503. [CrossRef]

[40]   Khashi'ie NS, Arifin NM, Hafidzuddin EH, Wahi N. Thermally stratified flow of Cu-Al$_2$O$_3$/water hybrid nanofluid past a permeable stretching/shrinking circular cylinder. J Adv Res Fluid Mech Therm Sci 2019;63:154−163.

[41]   Chung JD, Ramzan M, Gul H, Gul N, Kadry S, Chu YM. Partially ionized hybrid nanofluid flow with thermal stratification. J Mater Res Technol 2021;11:1457−1468. [CrossRef]

[42]   Shampine LF, Kierzenka J, Reichelt MW. Solving boundary value problems for ordinary differential equations in MATLAB with bvp4c. Tutorial Notes 2000;2000:1−27.

[43]   Kierzenka J, Shampine LF. A BVP solver based on residual control and the Maltab PSE. Trans Math Softw 2001;27:299−316. [CrossRef]

[44]   Ishak A, Nazar R. Laminar boundary layer flow along a stretching cylinder. Europ J Sci Res 2009;36:22−29.

[45]   Elbashbeshy EM, Emam TG, El-Azab MS, Abdelgaber KM. Laminar boundary layer flow along a stretching cylinder embedded in a porous medium. Int J Phys Sci 2012;7:3067−3072. [CrossRef]